

Movement of Palladium Nanoparticles in Hollow Graphitised Nanofibres: the Role of Migration and Coalescence in Nanocatalyst Sintering during the Suzuki-Miyaura Reaction

Received 00th January 20xx,
Accepted 00th January 20xx

DOI: 10.1039/x0xx00000x

Rhys. W. Lodge,^[a] Graham. A. Rance,^[a,b] Michael. W. Fay^[b] and Andrei. N. Khlobystov^{*,[a,b]}

The evolution of individual palladium nanoparticle (PdNP) catalysts, in graphitised nanofibres (GNF), in the liquid-phase Suzuki-Miyaura (SM) reaction has been appraised. The combination of identical location-transmission electron microscopy (IL-TEM) and a nano test tube approach allowed spatiotemporal continuity of observations at single nanoparticle level, revealing that migration and coalescence is the most significant pathway to coarsening of the nanocatalyst, rather than Ostwald ripening. IL-TEM gave unprecedented levels of detail regarding the movement of PdNP on carbon surfaces at the nanoscale, including size-dependent migration and directional movement, opening horizons for optimisation of future catalysts through surface morphology design.

Introduction

The palladium-catalysed Suzuki-Miyaura (SM) cross-coupling of an organoboronic acid and an organohalide is one of the most important, and versatile, reactions utilised for the formation of carbon-carbon bonds in the synthesis of a wide range of anti-cancer agents, natural products and other structurally-complex motifs.^[1-3] The application of supported palladium nanoparticles (PdNP) as catalysts of cross-coupling reactions has been rapidly increasing in recent times,^[4-5] exploiting the high surface area to volume ratio and low coordination number of surface atoms in PdNP^[6-8] and the ease of extraction and recyclability of the catalyst.^[9-11] However, the highly dynamic nature of metal nanoparticles often leads to increasing nanoparticle sizes during catalytic cycles, which decreases the number of active surface atoms and reduces catalytic activity.^[12-14] Consequently, there has been a significant drive to better understand the fundamental mechanisms (Figure S1) that lead to undesired nanoparticle growth and deactivation – with the majority of reports identifying Ostwald ripening as the most important factor in particle coarsening – and thus guide the development of novel nanoscale materials where these disadvantageous processes are inhibited.^[15-17] Although a multitude of microscopy techniques have previously been used to appraise the growth of nanoparticles, one of the most widely utilised is transmission electron microscopy (TEM), with two specific imaging strategies, namely the sampling (Figure 1A, S2) and *in-situ* environmental TEM (ETEM) methods (Figure S3), commonly employed.^[18-21] The sampling methodology involves

inspection of the size and shape of nanoparticles before and after the reaction and conclusions are drawn by averaging their structural characteristics over the ensemble.^[22,23] However, whilst the sampling technique is simplistic, it is limited by its inability to relocate unique regions of a sample between treatments. As a consequence, the spatiotemporal continuity for assessing the dynamics of individual nanoparticles cannot be achieved and, thus atomistic mechanisms leading to any observed changes in the catalyst remain unknown, if the identity of nanoparticles is not preserved throughout the process.^[24,25] With ETEM, specialist sample holders allow for individual nanoparticles to be imaged or filmed with atomic resolution under elevated temperatures and gaseous environments, providing mechanistic details under realistic working conditions.^[26-28] However, in ETEM analysis there is typically a compromise between imaging the sample to obtain the required information and preventing electron beam damage to the material.^[29] Additionally, the efficacy of ETEM for liquid-phase reactions is hindered by: i) strong interactions of the e-beam with material of the sample holder window and solvent molecules, precluding high resolution imaging; ii) the formation of radical species from the solvent, due to knock-on damage, causing a divergence from realistic reaction conditions; and iii) liquid-phase reaction times often occurring over extended time periods.^[30-32]

Simple TEM imaging of nanocatalysts before and after a reaction (Figure 1A) cannot explain how and why the sintering process occurs due to the inherent non-uniformity of

^aSchool of Chemistry, University of Nottingham, University Park, Nottingham NG7 2RD, UK

^bNanoscale and Microscale Research Centre, Cripps South, University of Nottingham, University Park, Nottingham NG7 2RD, UK.

*Corresponding author email address: andrei.khlobystov@nottingham.ac.uk

Electronic Supplementary Information (ESI) available: See DOI: 10.1039/x0xx00000x

nanoparticles. However, identical location TEM (IL-TEM) – pioneered by Mayrhofer *et al.*^[33] nearly a decade ago, where the material is deposited onto a finder grid, analysed, exposed to selected reaction conditions, and then re-analysed in a location identical to that prior to the reaction (Figure 1B) – is a further TEM analysis method which critically enables direct evaluation of individual nanoparticle evolution in *ex-situ* liquid-phase reactions (Table S1). Yet, to the best of our knowledge, the application of IL-TEM is currently limited to studying the coarsening of nanoparticles in electrocatalytic chemical reactions.^[34–37] In this study, we combine the IL-TEM strategy with our nano test tube approach to provide a powerful methodology enabling preservation of the spatial continuity of nanocatalyst observation in preparative, liquid-phase, cross-coupling reactions with nanoscale precision. Surprisingly, we revealed that PdNP undergo migration and coalescence during catalysis of the SM reaction, rather than increasing their size through dissolution-precipitation or Ostwald ripening which are commonly accepted key mechanisms of nanocatalyst sintering.

Moreover, we show that the migration of PdNP appears to be dependent on their size and position on the support.

Entrapment of catalyst nanoparticles within carbon nano test tubes, such as carbon nanotubes (CNT) and hollow graphitised nanofibres (GNF) (Figure 1C, D and E) permits effective control of the activity, selectivity and recyclability of nanocatalysts,^[38–41] whilst providing improved manoeuvrability and an excellent imaging platform for single-particle analysis by TEM. We combined and exploited all of these aspects in this study by selectively depositing PdNP within the GNF (PdNP@GNF).^[42] Thus formed nanoparticles of metallic palladium have an average diameter of 6.87 ± 3.20 nm ($N = 75$) with >80% deposited within the internal channel of GNF (Figure 1F, G and H). The corrugated interior of GNF produces regions known as step-edges that enable localisation of the nanoparticles (Figure 1)^[22,23] – ideal for catalytic reactions and subsequent analysis of individual, uniquely identifiable PdNP by IL-TEM.

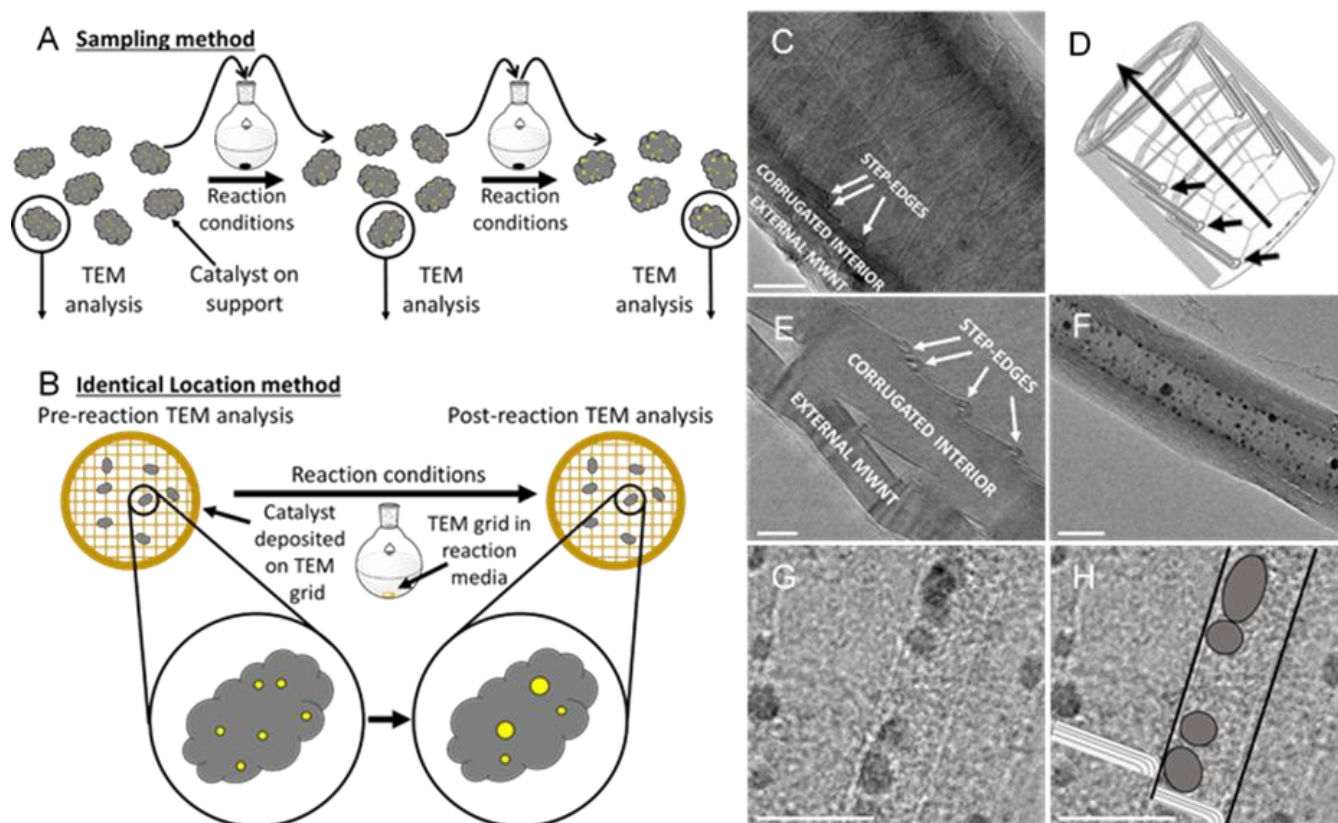


Figure 1. Schematics of the sampling (A) and IL-TEM (B) methods for the analysis of nanoparticle catalyst materials by TEM. Low and high magnification electron micrographs (C, E, F and G) and schematics (D and H) highlight the different internal and external structures of GNF. The internal step-edges provide effective anchoring points for metallic nanoparticles (G). A schematic overlaid on image G (H) highlights the step-edges (black lines) and shows that the nanoparticles (dark grey ellipses) are located adjacent to them, reflecting the maximization of van der Waals surface area and subsequent interactions. Scale bars are 20 nm (C), 5 nm (E), 50 nm (F) and 10 nm (G and H).

Experimental

Catalyst Preparation

PdNP@GNF preparation was carried out following the method outlined in Cornelio *et al.*^[42] Materials characterisation is reported in Section C of the supporting information file.

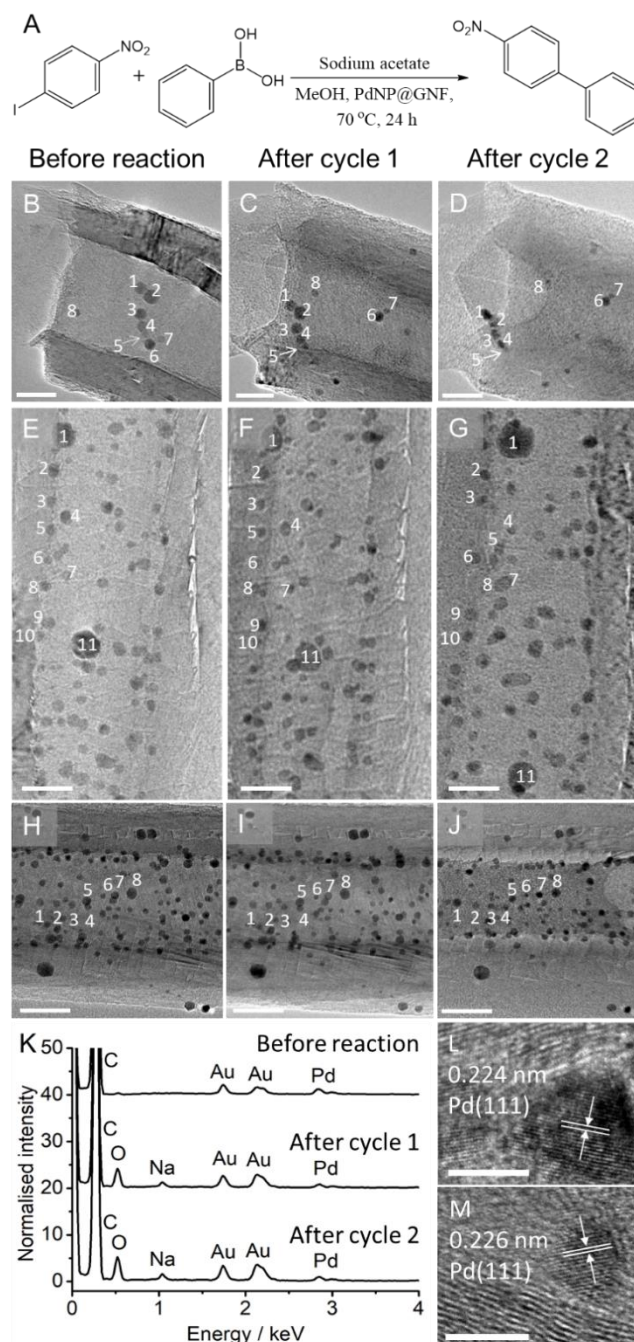
IL-TEM Experimental Procedure

Loading of the nanocatalyst onto the TEM grid for the IL-TEM experiments was carried out as follows: to PdNP@GNF (10 μg , 1 mol%) was added methanol (0.5 mL) and the resulting suspension was sonicated for 5 seconds. The suspension was deposited onto a gold mesh, graphene oxide on lacey carbon film TEM finder grid (EM Resolutions) suspended between tweezers, allowing for solvent evaporation between drops, until all the suspension had been deposited. The SM reaction conditions were obtained from Cornelio *et al.*^[42] In a typical reaction for the IL-TEM experiments, to 4-iodonitrobenzene (14.0 mg, 0.056 mmol, 1 eq.) in a two-necked round-bottomed flask was added, phenyl boronic acid (8.9 mg, 0.073 mmol, 1.3 eq), sodium acetate (10.6 mg, 0.13 mmol, 2.3 eq.) and the PdNP@GNF/TEM finder grid. A degassed solution of methanol (5 mL) was added *via* cannula and the resulting suspension heated under an inert atmosphere of argon at 70 °C for 24 h with no stirring. The TEM grid was removed and left to dry under ambient conditions. The solvent was removed *in vacuo* and the resulting solid analysed by ¹H NMR spectroscopy (Bruker DPX-300, 300 MHz, CDCl₃) for determination of TOF. TEM was performed using a JEOL 2100F transmission electron microscope with an accelerating voltage of 200 kV (field emission electron gun source, information limit 0.19 nm). EDX spectroscopy was performed using an Oxford Instruments XMax 80 T silicon drift detector with INCA Energy 250 Microanalysis system.

Results and Discussion

Although the conventional sampling approach (Figure 1A) cannot provide any specific information for individual nanoparticles, using PdNP@GNF deposited on a TEM finder-grid allows for changes in individual nanoparticles to be monitored subsequent to immersion in a liquid reaction mixture by TEM. Interestingly, we found that the TEM grid composition, including both the film upon which PdNP@GNF is mounted and the metallic grid mesh that supports the film itself, is of critical importance. Systematic analysis of a variety of film (SiO₂/formvar, graphene oxide/lacey carbon and lacey carbon) and mesh (Cu and Au) combinations after exposure to the conditions of a typical SM reaction indicated that a graphene oxide on lacey carbon film supported on a gold mesh was the most suitable for IL-TEM analysis (Section D, SI). With the optimum composition identified, the IL-TEM experiments were performed as follows: (i) PdNP@GNF were deposited onto the finder grid and analysed by TEM (Figure 2B, E and H); (ii) the TEM grid, supporting the nanoreactor catalyst, was placed into a round-bottom flask containing 4-iodo-1-nitrobenzene, phenyl boronic acid, sodium acetate and methanol and the mixture heated with no agitation for 24 h at 70 °C; (iii) the grid was carefully removed from the flask and analysed by TEM (Figure 2C, F and I); (iv) the procedure was repeated (Figure 2G and J). To ensure the PdNP were catalytically active in the SM reaction, the reaction mixture was analysed by ¹H NMR spectroscopy after removal of the TEM grid from the reaction flask; a calculated turnover frequency (TOF) based on the available

active sites of $4.2 \times 10^4 \text{ h}^{-1}$ was determined. A TOF value based on mol% of catalyst of $0.1 \text{ mol mol}^{-1} \text{ h}^{-1}$ was additionally calculated and found to be similar to both that observed in the bulk preparative reactions using our current catalyst (Section E,



SI) and to that reported previously.^[42]

Figure 2. The Suzuki Miyaura reaction (A) and a series of TEM images comparing PdNP@GNF nanoreactors as prepared (B, E and H) and after their first (C, F and I) and second use (D, G and J) in the Suzuki-Miyaura reaction. Further analysis beyond the second use is complicated by the fragility of current TEM grids. Nanoparticle migration was observed in all cases, with some numbered to aid their identification. Amorphous material was noted within the internal channel of the nanofibres, attributed to solvent and reactant molecules (C, D and J). The mean diameter of nanoparticles imaged in panels B – D were 5.52 ± 1.31 , 5.60 ± 1.32 nm and 5.59 ± 1.33 nm ($N = 8$, pixel width = 0.13 nm), respectively. This indicates that no growth had occurred in this region and highlights the issue of sole statistical treatment of images in that specific information relating to movement and growth of nanoparticles may be lost. In addition to carbon and palladium, EDX spectroscopy of the PdNP@GNF in panels E – G confirmed the presence of sodium and oxygen, attributed to the sodium acetate base used in the reaction (J) (gold originated from the mesh of the TEM grid). No change in the interplanar d-spacing

obtained by HR-TEM from different PdNPs before the first (L) and after the second use (M) confirmed that the oxygen observed in the EDX spectra was not due to oxidised PdNP. Scale bars are 20 nm (B – G), 50 nm (H – J) and 5 nm (L and M).

Comparing TEM images of PdNP@GNF prior to and after one and two uses (Figure 2B – J), the IL-TEM methodology allows the fate of individual PdNP to be followed by directly imaging their positions and sizes. IL-TEM imaging revealed that, from one reaction cycle to another, the nanoparticles do not dissolve or move far away from their original locations meaning individual NPs can be numbered and reliably monitored. Investigation of the particle size evolution indicates no significant contribution of Ostwald ripening under the SM reaction conditions, which has a distinct signature of smaller particles decreasing and larger particles increasing in size.^[43] Indeed, careful analysis of the nanoparticles encircled in Figure 3A and B shows smaller nanoparticles in the vicinity of a larger one increasing in size after exposure to the reaction conditions, thus providing clear evidence of nanoparticle migration and coalescence controlling the coarsening dynamics. The observation of organic material within the nanofibre (Figure 3B, dashed white line,) is due to reactant and solvent molecules, thus confirming their accessibility to the catalyst nanoparticles.

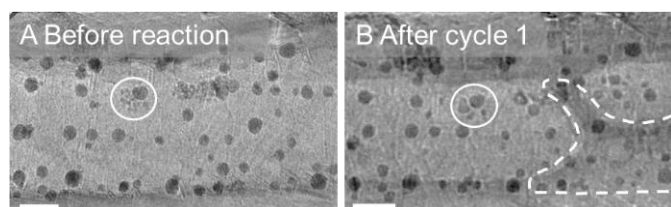


Figure 3. An increase in the size of small PdNPs (A) after cycle 1 (B) was noted, indicating that particle migration and coalescence accounts for PdNP coarsening. No obvious increase in the size of the larger adjacent nanoparticle would appear to rule out the role of Ostwald ripening under these conditions. The region of contrast highlighted by the dashed white line shows that the reagents were able to access the internal cavity of the GNF. Scale bars are 20 nm.

As migration appeared to be the main type of PdNP dynamics, IL-TEM allowed us to study the directionality of nanoparticle movement: smaller nanoparticles (<5 nm in size) exhibited short-range (<20 nm) transverse migrations perpendicular to the GNF long axis (Figure 4Ai, particles 6 and 7 between Figure 2B and C), but larger nanoparticles (>5 nm) displayed long-range, longitudinal migrations parallel to the GNF long axis (Figure 4Aiii), in some cases by up to 50 nm (particle 11 between Figure 2F and G). The size-dependent migrations can be explained by the extent of van der Waals interactions between nanoparticles and the graphitic step-edges of GNF, exploited in preparative catalysts in our previous works.^[38–41] Nanoparticles with smaller diameters than the height of the step-edge (<5 nm) have an excellent geometric fit, maximising van der Waals contact and consequently limiting migration to predominantly transverse motion around the circumference of the GNF (Figure 4B) and, in some instances, a short-range longitudinal motion down the graphitic step-edge, but critically not over the step-edge. In contrast, nanoparticles larger than the step-edge (Figure 4B) have a poorer geometric fit leading to weaker van der Waals interactions and subsequently less restricted migration (crossing more than eight step-edges in the case of particle 11 between Figure 2F and G), without preferential direction. Importantly, as Ostwald ripening does not appear to

be significant, our observation of size-dependent migrations would suggest that growth of PdNP can be totally inhibited by enhancing van der Waals interactions between PdNP and the support material to such an extent that growth by particle migration and coalescence also becomes unfavourable, thus leading to a durable palladium nanocatalyst for wide range of preparative cross-coupling reactions.

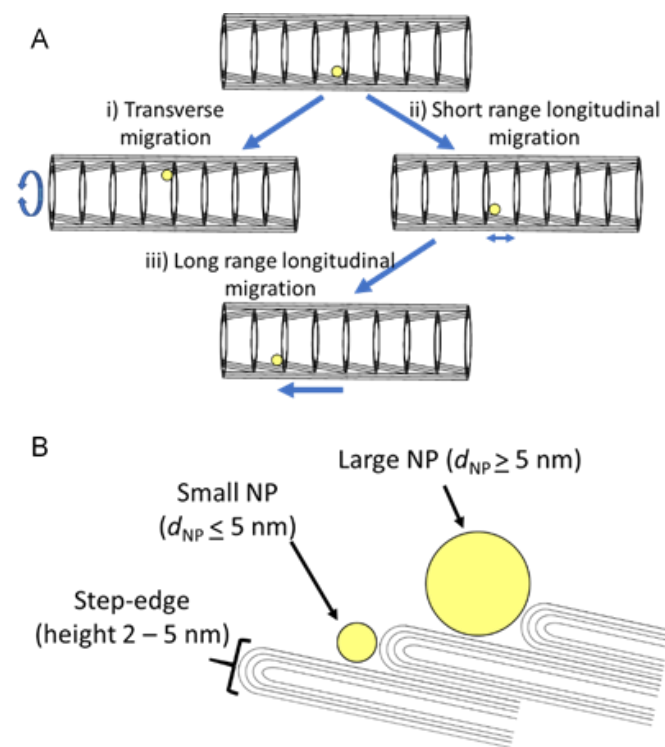


Figure 4. Schematics of PdNP migration in graphitised nanofibres. The observed behaviour can be explained by looking at the direction the nanoparticle has travelled. Particles can exhibit transverse movement along the step-edge, perpendicular to the growth axis of the nanofibre (Ai) or move away from the step-edge, parallel to the growth axis of the nanofibre, if the van der Waals interaction is not sufficient, in short range longitudinal migration (Aii). If the nanoparticle has sufficient energy to undergo long range longitudinal migration (Aiii) it can move down to the next step-edge. To reverse this process would require sufficient energy to traverse the step-edge which is unlikely to happen because it is an energetically unfavourable process. The size of the nanoparticles, with respect to the step-edge, determines the strength of their van der Waals interaction with smaller nanoparticles possessing a better geometric fit relative to larger nanoparticles (B).

Conclusions

In summary, we have successfully applied an innovative combination of IL-TEM analysis and the nano test tube approach to investigate the behaviour of supported metal nanoparticles as catalysts of liquid-phase, preparative reactions. We have solved the inherent practical challenges associated with IL-TEM analysis of nanocatalysts used in liquid reactions and developed a method that can provide not only structural information on individual nanocatalysts, but complementary local-probe chemical analysis by means of EEL and EDX spectroscopy. We have demonstrated that IL-TEM analysis of PdNP within GNF allows the evolution of individually identifiable nanoparticles to be tracked, demonstrating that PdNP remain solid during the reaction (i.e. do not dissolve and re-precipitate as commonly perceived), and that nanoparticle

migration and coalescence is the principle mechanism decreasing the active surface area under the conditions of the Suzuki-Miyaura reaction. These results suggest that the pseudo-homogeneous mechanism proposed for palladium and other metal nanoparticles, through dissolution-precipitation events, may not be as prevalent as expected from previous studies using the sampling approach,^[25] thus highlighting the importance of IL-TEM for providing key mechanistic insights for nanocatalysis. Furthermore, the spatiotemporal continuity of IL-TEM allows to monitor the evolution of uniquely defined nanoparticles, imaged before and after the reaction cycles, clearly indicated that Ostwald ripening – the most widely cited, but hardest to control, mechanism of nanoparticle growth – is not solely responsible for the nanoparticle coarsening observed under the investigated reaction conditions. Moreover, we have shown that the graphitic step-edges of the nanofibres were essential for determining the direction and magnitude of nanoparticle migration during catalysis. Two different migrational modes – longitudinal (parallel to the long axis of the nanofibre) and transverse (perpendicular to the long axis of the nanofibre) – were identified, with a clear size-dependence to these migrations observed. Insights gained from our observations on the relationship between the growth and migration of nanoparticles and the morphology of the graphitic surface offers a powerful strategy for engineering highly durable carbon supports, with step-edges matching the size of catalytic centres. This may ultimately lead to the inhibition of nanoparticle growth and subsequent deactivation as coarsening by particle migration and coalescence can effectively be controlled in such a fashion. As such, we offer new hope for the development of future nanocatalytic materials, particularly those applicable to environmentally- and economically-sustainable chemical synthesis.

Conflicts of interest

There are no conflicts to declare.

Acknowledgements

The authors acknowledge the Nanoscale and Microscale Research Centre (nmRC) at the University of Nottingham for access to the TEM facilities and EPSRC for funding.

Notes and references

- S. R. Chemler, D. Trauner and S. J. Danishefsky, *Angew. Chem. Int. Ed.*, 2001, **40**, 4544-4568.
- H. Wang, Z. Yan, W. Lei, K. Sheng, Q. Yao, K. Lu, and P. Yu, *Tetrahedron Lett.*, 2014, **55**, 897-899.
- A. Petran, A. Terec, E. Bogdan, A. Soran, E. Lakatos and I. Grosu, *Tetrahedron*, 2014, **70**, 6803-6809.
- D. Sahu, A. Silva, and P. Das, *Catal. Commun.*, 2016, **86**, 32-35.
- N. Huang, Y. Xu and D. Jiang, *Sci. Reports*, 2014, **4**, 7228.
- B. S. Kumar, A. J. Amali and K. J. Pitchumani, *J. Mol. Catal. A: Chem.*, 2016, **423**, 511-519.
- L. Yu, and Z. Han, *Mater. Lett.*, 2016, **184**, 312-314.
- S. Rana, S. Maddila, K. Yalagala and S. B. Jonnalagadda, *Appl. Catal., A*, 2015, **505**, 539-547.
- T. Borkowski, W. Zawartka, P. Pospiech, U. Mizerska, A. M. Trzeciak, M. Cypriak, and W. Tylus, *J. Catal.*, 2011, **282**, 270-277.
- X. Le, Z. Dong, Y. Liu, Z. Jin, T.-D. Huy, M. Le, and J. Ma, *J. Mater. Chem. A*, 2014, **2**, 19696-19706.
- Y. Li, L. Xu, B. Xu, Z. Mao, H. Xu, Y. Zhong, L. Zhang, B. Wang and X. Sui, *ACS Appl. Mater. Interfaces*, 2017, **9**, 17155-17162.
- S. G. Rinaldo, W. Lee, J. Stumper and M. Eikerling, *Physical Review E*, 2012, **86**, 041601.
- L. Shang, T. Bian, B. Zhang, D. Zhang, L.-Z. Wu, C.-H. Tung, Y. Yin and T. Zhang, *Angew. Chem. Int. Ed.*, 2014, **53**, 250-254.
- H.-H. Zhang, B. Liu, J. Wang, K. Feng, B. Chen, C.-H. Tung and L.-Z. Wu, *Tetrahedron*, 2014, **70**, 6188-6192.
- M. Pérez-Lorenzo, *J. Phys. Chem. Lett.*, 2012, **3**, 167-174.
- T. W. Hansen, A. T. DeLaRiva, S. R. Challa and A. K. Datye, *Acc. Chem. Res.*, 2013, **46**, 1720-1730.
- I. V. Yentekakis, G. Goula, P. Panagiotopoulou, S. Kampouri, M. J. Taylor, G. Kyriakou, and R. M. Lambert, *App. Catal. B*, 2016, **192**, 357-364.
- R. Anton, and I. Schneidereit, *Phys. Rev. B*, 1998, **58**, 13874-13881.
- A. Kolmakov and D. W. Goodman, *Surf. Sci.*, 2001, **490**, L597-L601.
- D. E. Starr, S. K. Shaikhutdinov and H.-J. Freund, *Top. Catal.*, 2005, **36**, 33-41.
- E. Longo, W. Avansi Jr., J. Bettini, J. Andrés and L. Gracia, *Sci. Rep.*, 2016, **6**, 21498.
- B. Cornelio, G. A. Rance, M. Laronze-Cochard, A. Fontana, J. Sapi and A. N. Khlobystov, *J. Mater. Chem. A*, 2013, **1**, 8737-8744.
- W. A. Solomonsz, G. A. Rance, B. J. Harris and A. N. Khlobystov, *Nanoscale*, 2013, **5**, 12200-12205.
- A. K. Datye, Q. Xu, K. C. Kharas and J. M. McCarty, *Catal. Today*, 2006, **111**, 59-67.
- E. D. Goodman, J. A. Schwalbe and M. Cargnello, *ACS Catal.*, 2017, **7**, 7156-7173.
- S. B. Vendelbo, C. F. Elkjær, H. Falsig, I. Puspitasari, P. Dona, L. Mele, B. Morana, B. J. Nelissen, R. van Rijn, J. F. Creemer, P. J. Kooyman and S. Helveg, *Nat. Mater.*, 2014, **13**, 884-890.
- H. Yoshida, Y. Kuwauchi, J. R. Jinschek, K. J. Sun, S. Tanaka, M. Kohyama, S. Shimada, M. Haruta and S. Takeda, *Science*, 2012, **335**, 317-319.
- R. Wang, P. A. Crozier and R. Sharma, *J. Phys. Chem. C*, 2009, **113**, 5700-5704.
- M. Ek, S. P. F. Jespersen, C. D. Damsgaard and S. Helveg, *Adv. Struct. Chem. Imag.*, 2016, **2**, 4.
- F. Tao and P. A. Crozier, *Chem. Rev.*, 2016, **116**, 3487-3539.
- N. M. Schneider, M. M. Norton, B. J. Mendel, J. M. Grogan, F. M. Ross and H. H. Bau, *J. Phys. Chem. C*, 2014, **118**, 22373-22382.
- S. B. Simonsen, I. Chorkendorff, S. Dahl, M. Skoglundh, J. Sehested and S. Helveg, *J. Catal.*, 2011, **281**, 147-155.
- K. J. J. Mayrhofer, S. J. Ashton, J. C. Meier, G. K. H. Wiberg, M. Hanzlik, and M. Arenz, *J. Power Sources*, 2008, **185**, 734-739.
- K. J. J. Mayrhofer, M. Hanzlik and M. Arenz, *Electrochim. Acta*, 2009, **54**, 5018-5022.
- K. Hartl, M. Hanzlik, and M. Arenz, *Energy Environ. Sci.*, 2011, **4**, 234-238.
- F. Nikkuni, L. Dubau, E. A. Ticianelli and M. Chatenet, *Appl. Catal., B*, 2015, **176-177**, 486-499.
- C. Baldizzone, L. Gan, N. Hodnik, G. Keeley, A. Kostka, M. Heggen, P. Strasser and K. J. J. Mayrhofer, *ACS Catal.* 2015, **5**, 5000-5007.
- M. C. Gimenez-Lopez, A. Kurtoglu, D. A. Walsh and A. N. Khlobystov, *Adv. Mater.*, 2016, **28**, 9103-9108

- 39 W. A. Solomonsz, G. A. Rance and A. N. Khlobystov, *Small*, 2014, **10**, 1866-1872.
- 40 G. A. Rance, W. A. Solomonsz, and A. N. Khlobystov, *Chem. Commun.*, 2013, **49**, 1067-1069.
- 41 A. N. Khlobystov, *ACS Nano*, 2011, **5**, 9306-9312.
- 42 B. Cornelio, A. R. Saunders, W. A. Solomonsz, M. Laronze-Cochard, A. Fontana, J. Sapi, A. N. Khlobystov and G. A. Rance, *J. Mater. Chem. A*, 2015, **3**, 3918-3927.
- 43 S. B. Simonsen, I. Chorkendorff, S. Dahl, M. Skoglundh and S. Helveg, *Surf. Sci.*, 2016, **648**, 278-283.